IEEE Access
Multidisciplinary | Rapid Review | Open Access Journal

Received 10 April 2023, accepted 21 April 2023, date of publication 28 April 2023, date of current version 4 May 2023.

Digital Object Identifier 10.1109/ACCESS.2023.3271516

RESEARCH ARTICLE

Robust Estimates of the Total Alkalinity From Satellite Oceanographic Data in the Global Ocean

KANDE VAMSI KRISHNA AND PALANISAMY SHANMUGAM
Ocean Optics and Imaging Laboratory, Department of Ocean Engineering, Indian Institute of Technology Madras, Chennai 600036, India

Corresponding author: Palanisamy Shanmugam (pshanmugam@iitm.ac.in)

This work was supported in part by the Ministry of Human Resources and Development (MHRD), and in part by the National Geospatial Program (NGP) of the Department of Science and Technology of Government of India under Grant OEC1819150DSTXPSHA.

ABSTRACT Total alkalinity (TA) is a key parameter to understand the dynamics of biogeochemical properties in the global ocean and the effects of climate change on ocean acidification, ocean carbon cycle, and carbonate chemistry. To date, global surface ocean distributions of TA were investigated using multiple regional regression approaches which require smoothening techniques due to severe boundary effects in different oceanic regions/basins across latitudes/longitudes. To reduce the uncertainties and produce spatially and temporally consistent TA products, a novel single linear regression (SLR) approach was developed in this study to estimate TA fields in the global surface ocean waters. The SLR formulation was derived using the continuous in-situ measurements of sea surface salinity (SSS) collected from the different oceans. The performance of the SLR was assessed using independent in-situ/satellite derived TA data and the results from three existing algorithms. In general, the SLR-based global surface ocean TA fields from both in-situ and satellite data agreed well with in-situ measured TA data with a mean relative error less than 1%, which is much lower compared to the error with the existing algorithms. Studies were also conducted to examine the spatiotemporal variability and trends in the global surface ocean climatology of SSS and TA fields in the context of current climate change impacts.

INDEX TERMS Total alkalinity, sea surface salinity, carbon chemistry, global ocean, satellite data.

I. INTRODUCTION

Ocean total alkalinity (TA expressed in a unit of μmol kg^{-1}) is expressed as the excess of bases (proton acceptors) over acids (proton donors). It provides an unprecedented opportunity, particularly when combined with sea surface salinity (SSS), for studying carbon cycle, air-sea CO_2 fluxes, ocean acidification and carbonate chemistry [1], [2], [3]. In general, the spatiotemporal variability of global surface ocean TA was linked to the various physical (evaporation and precipitation), biological (photosynthesis and oxidation of organic matter) and non-conservative processes (production and dissolution of $CaCO_3$) [2], [4], [5]. Earlier studies have demonstrated that TA is largely controlled by SSS [6], as evident from the strong linear correlation between SSS and TA [5], [7], [8]. This formed the basis of earlier studies to derive multiple regional regression equations to estimate surface ocean TA as a function of SSS. Using this approach, Sarma [7] estimated surface ocean TA in Arabian Sea waters with RMSE $\pm$5.7 μmol kg^{-1}. In another study, Sarma et al. [8] estimated surface ocean TA with RMSE $\pm$4.8 μmol kg^{-1}. In Northwest Atlantic Ocean water, Cai et al. [9] established the relationship between TA and SSS with RMSE 21.6 μmol kg^{-1}. In the western tropical Atlantic (WTA) region, Lefévre et al. [10] constructed a TA relationship as a function of the SSS with a RMSE deviation of 11.6 μmol kg^{-1}. Takatani et al. [11] proposed five regional equations for the surface Pacific Ocean waters based on the relationships between TA, SSS and sea surface dynamic heigh (SSDH) which yielded a RMSE $\pm$7.8 μmol kg^{-1}. Arrigo et al. [12] established TA relationships as a function of the SST and SSS in the Arctic surface ocean waters with RMSE 26.9 μmol kg^{-1}.

In the Southern Ocean region, McNeil et al. [13] estimated surface ocean TA as a function of the SSS, nitrate and silicate

The associate editor coordinating the review of this manuscript and approving it for publication was Geng-Ming Jiang.

concentrations. Bates et al. [14] examined the spatiotemporal variability of upper ocean TA in the Indian Ocean using SST, SSS, apparent oxygen utilization (AOU), latitude, depth, nitrate and phosphate concentrations. Various methods have been adopted to build the spatiotemporal gaps in TA observations to produce the global seasonal climatological maps. Millero et al. [5] developed the first set of global TA relationships by dividing the world's oceans into six regions, and parametrized the SSS normalized TA with SST using in-situ measured surface TA data (N = 1740). Due to the SSS normalization of inorganic carbon (TA) chemical data, Millero et al. [5] established a relationship between TA and SST which included the erroneous trends [15]. Since the global TA relationship became available, Lee et al. [3] added a significant new number of TA measurements (N = 5692), grouped TA data (<20-30m depth), divided these data into the five ocean regions, and obtained the best fits through the SST and SSS quadratic functions for each regions.

According to Lee et al. [3], TA is estimated from satellite derived SST and SSS data using the locations (latitudes and longitudes) and ranges of SST and SSS for the different oceanographic regions. Lee et al. [3] probably included some uncertainties/errors due to seasonal variations. When changing the specified ranges of SST and SSS for each region and including the additional ''longitude'' parameter, there was an overestimation of TA in North Pacific waters [2]. Millero et al. [5] and Lee et al. [3] estimated ocean surface TA based on SSS and SST data without the inclusion of parameters representing the net community production. To overcome this problem, Takahashi et al. [4] classified the world's ocean into 33 regions and estimated the potential alkalinity (PALK = TA+NO_3^-) of 27 regions as a linear function of SSS. To eliminate the seasonal biological effects (due to organic production and utilization) and contributions of horizontal and vertical mixed waters (due to upwelling of deep water), this scheme used PALK instead of TA. Takahashi et al. [4] excluded the coastal regions and equatorial pacific zones from their analysis due to the large irregular intra- and inter-annual variabilities in the dynamic oceans.

Estimation of the spatiotemporal variability of surface ocean TA in global ocean waters is generally a challenge with the regional approaches due to the multiple relationships covering the various spatial (regions) and temporal (seasonal) scales would have severe boundary discontinuity problems across latitudes/longitudes and ocean basins [16]. To overcome these problems, few recent studies attempted to estimate TA globally without the boundaries. For example, Sasse et al. [17] constructed a non-linear regression algorithm to estimate TA in global ocean mixed layers as a function of the temperature, salinity, dissolved oxygen and nutrients concentrations. Similarly, Carter et al. [18] developed a locally interpolated alkalinity regression (LIARv2) approach. Recently, Broullón et al. [19] produced global monthly TA climatological products using a high potential feed-forward neural network approach with RMSE 5.1 μmol kg^{-1}. More recently, Gregor and Gruber [20] developed geospatial random cluster ensemble regression (GRaCER) approach to construct the global monthly climatological TA maps at a 1° × 1° spatial resolution over the period from 1985-2018, because of their potential applications for ocean acidification studies (ocean satellite oceanographic datasets for acidification - OceanSODA). Although, these algorithms improved surface ocean TA estimations in global ocean regions, but difficult to implement on the satellite data due to the complexity in model formulations.

To overcome such issues and limitations, this study developed a single linear regression (SLR) algorithm to estimate global oceanic surface TA as a function of the SSS from continuous in-situ measurement data (N = 11952). Although multiple in-situ and satellite-based approaches have been developed on estimating the spatiotemporal variability of surface ocean TA fields by considering the complex physical and biogeochemical parameters, the present SLR approach is more robust and accurate in estimating TA from the satellite-derived SSS products for the global region. The rationale for this SLR approach is that SSS is closely linked to the concentration of dissolved ions in seawater (including bicarbonate and carbonate ions), which are the major components of TA. Therefore, SSS serves as a proxy for TA in the global ocean. Additionally, the relationship between TA and SSS is relatively more stable over the time and space in the open oceans, which allows for accurate estimates of TA to be made even in areas where direct measurements are not available. Finally, the global ocean is a large and well-mixed system, meaning that the variation in TA and SSS fields is relatively small compared to the overall range of values. This can make it easier to identify and derive a relationship between these two variables using the SLR approach. Global surface ocean TA estimation using the single global algorithm has advantage of generating different spatial and temporal TA maps without the need of smoothing techniques between different oceanic regions/basins [19]. The new SLR algorithm is simple in a mathematical and physical perspective and more robust than the earlier approaches in estimating TA with an improved accuracy. This SLR approach is validated using independent in-situ measurement data and its applicability for the global ocean is demonstrated using satellite-derived SSS data and the previously reported TA data products with a spatial resolution of 1° × 1° for the reference year 2014 [4].

II. DATA

A. IN-SITU DATA

Global ocean surface in-situ measurements of TA and SSS for model development and validation were obtained from the Ocean Acidification Data Stewardship (OADS) data management project within the National Oceanic and Atmospheric Administration (NOAA) - National Centers for Environmental Information (NCEI) (https://www.ncei.noaa.gov/access/oads/), which provides highly quality controlled, more precise and accurate data for the purpose of developing and

TABLE 1. OADS in-situ data used for deriving the SLR formulation.

Ocean region	Date	N	Latitude and Longitude	Vessel name	Observer
Equatorial and North Pacific	1-6 Feb. 1998, 25-30 Mar. 1999 16-31 Oct. 1999,1-18 & 21-30 Nov. 1999,1-25 Dec. 1999, 9-31 Jan. 2001, 2-6 & 16-28 Feb. 2001, 1-22 Mar. 2001, 8-31 Jan. 2002, 1-14 & 22-28 Feb. 2002, 1-29 Mar. 2002, 16-22 Nov. 2002, 12-31 Dec. 2002 3-6 & 11-31 Jan. 2003, 2-12 Feb. 2003	5598	5.1S-39.78N 179.99W-179.99E	R/V Mirai	M. Ishii
Equatorial and North Atlantic	4-26 Sep. 2005, 27-31 May 2006, 2-14 & 20-29 June 2006, 1 & 19-30 Nov. 2006 6-30 June 2007, 1-3 July 2007, 3-24 Sep. 2007	159	10S-6.05N 12.56W-8E	ATALANTE	N. Lefèvre
North Atlantic	3-10 Oct. 2001	469	38.32N-55.55N 15.68W-8.8W	R/V Marion Dufresne	N. Metzl
Indian and Southern	15-31 Jan. 2000, 1-7 Feb. 2000, 19-31 July 2000, 1-13 June 2000, 3-10 Sep. 2001, 6-13 Jan. 2008, 1-2 Feb. 2008, 7-31 Jan. 2015, 2-7 Feb. 2015, 6-31 Jan. 2017, 1-6 Feb. 2017, 5-31 Jan. 2018, 1-9 Feb. 2018	5413	20.15S-58.60S 15.68W-83.27E	R/V Marion Dufresne	N. Metzl
Indian and Southern	8-18 Feb. 2016, 12-21 March 2016	86	28.50S-64.95S 76.65E-115.08E	R/V Roger Revelle	A. Dickson
North Atlantic	18-27 April 2006, 15-23 Oct. 2006	30	39.11N-62.91N 26.60W-71.68W	M/V Skogafoss	F. Millero
Atlantic and Indian	Jan. - Dec. 2007-2010	197	39.18S-43.14N; 94.41W-146.93E	M/V Pacific Celebes	D. Hydes and Z. Jiang

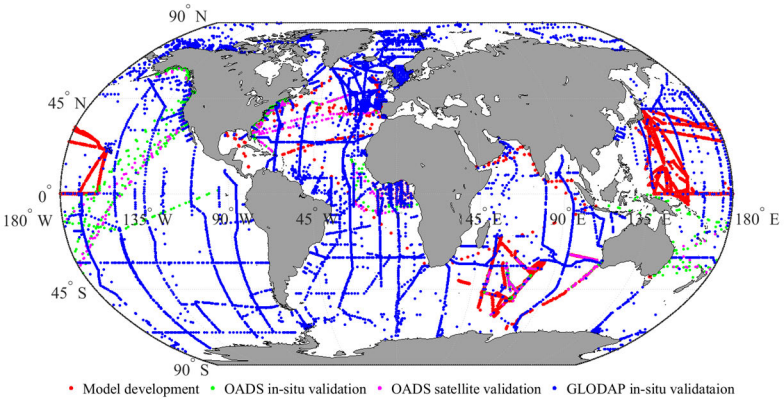

FIGURE 1. A map depicting the sampling locations and density of TA measurements in global and regional oceanic waters used in this study.

validating the various ocean algorithms. The primary and ancillary data are described in Tables 1 and 2 and their measurement locations are shown in Fig. 1. The training and validation datasets were extracted from the above database as a good representation of coastal and offshore waters in the Atlantic, Pacific and Southern oceans, which contain major tropical and subtropical domains, major gyre systems, warming and stratification conditions, mixing and dilution processes, and biological processes. The quality-controlled data of approximately 16949 samples (for the period 1998-2018) were split into two datasets with 11952 samples (approximately 70.51%, TA range: 2114-2463 μmol kg^{-1}, and SSS range: 32-37.7 PSU) for deriving the SLR algorithm and 4997 samples (~29.49%, TA range: 1861-2412 μmol kg^{-1}, and SSS range: 25.6-36.8 PSU) for validating the results. This is based on the spatiotemporal coverage and the satellite data availability (Aquarius, the entire Aquarius data records spans from 25 August 2011 to 7 June 2015; and SMAP, 7 July 2015 to present) (Tables 1 and 2). Although the model development dataset is large and covers the major coastal

TABLE 2. OADS in-situ data used for validating the SLR results.

Ocean region	Data	N	1°	Latitude and Longitude	Vessel name	Observer
North Atlantic	7-8 Mar. 2015, 28-30 Apr. 2015, 1-6 May. 2015, 16-24 Apr. 2016	84	68	19.28N-38.46N 10.39W-78.82W	M/V Equinox	R. Wanninkhof
Indian	8-12 Feb. 2016, 12-24 March 2016	53	47	28.50S-45.14S 96.05E-115.08E	R/V Roger Revelle	A. Dickson
North Atlantic	23-29 Aug. 2018	18	4	37.7N-41.47N 67.68W-74.57W	R/V Gordon Gunter	R. Wanninkhof
Indian	7-26 Jan. 2016, 10-28 Oct. 2016	542	79	30.02S-57.75S 52.30E-79.15E	R/V Marion-Dufresne	N. Metzl, C.L. Monaco
North Atlantic	25-30 June 2018, 1-29 July2018	161	35	26.95N-44.75N 61.39W-80.97W	R/V Henry Bigelow	W. J. Cai
North Atlantic	12-22 Feb. 2017	41	9	37.16N-42.50N 65.43W-75.95W	R/V Henry Bigelow	R. Wanninkhof
North Atlantic	11-21 Feb. 2017, 26-30 June 2018, 4-29 July 2018	2550	58	26.85N-43.77N 66.49W-80.97W	R/V Henry Bigelow	C. W. Hunt
North Atlantic	29-30 April 2017, 1-20 May 2017	82	30	42.07N-49.16N 11.44W-50.00W	R/V Celtic Explorer	P. Croot
North Pacific	18-28 Sep. 2017	190	8	44.19N-48.52N 127.01W-122.45W	Bell Shimada	M. L. Ostendorf, J. Herndon, S.R. Aline and R.A. Feely
Eastern Tropical Atlantic	10-29 April 2014, 1 & 5-16 May 2014, 18-30 March 2015, 1-15 April 2015, 8-29 March 2016, 8-11 April 2016, 26-28 Feb. 2017, 1-20 March 2017	144	86	9.92S-16N 24.65W-10.99E	R/V Le Suroit	N. Lefèvre
Pacific	17-31 July 2015	749	10	54.57N-60.29N 132.85W-156.59W	R/V Ronald Brown	J. Cross and N. M. Monacci
Pacific	Jan. – Dec. 2007-2012	383	88	48.51N-39.38S 179.84W-179.65E	R/V Ronald Brown	J. Cross and N. M. Monacci

and oceanic processes, the model validation dataset contains relatively a smaller number of samples with the limited spatial distribution across the global oceans. For more comprehensive testing of the algorithm, additional 10188 samples (depth < 5m, TA range: 1746-2468 μmol kg^{-1}, and SSS range: 25-37.6PSU) from the Global Ocean Data Analysis Project version2 (GLODAPv2) (https://www.glodap.info) was used for the validation analysis.

B. SATELLITE DATA

To demonstrate the robustness of SLR approach for deriving the spatiotemporal variability of global surface ocean TA, the global mapped Level-3 SSS products from the Aquarius sensor (spatial resolution: $1^\circ \times 1^\circ$ and temporal resolution: one week) were obtained from the National Aeronautics and Space Administration (NASA) - Goddard Space Flight Center (GSFC) (https://oceancolor.gsfc.nasa.gov). In addition, similar Level-3 SSS products from the Soil Moisture Active Passive (SMAP) sensor (spatial resolution: 70×70 km and temporal resolution: daily data files for this product are based on the SSS averages over an 8-day moving time window) were obtained from the NASA - Jet Propulsion Laboratory (JPL) (https://podaac.jpl.nasa.gov/SMAP). The NASA SeaWiFS Data Analysis System (SeaDAS) software was used to process satellite data (Aquarius and SMAP). For satellite validation analysis, matchups were established by averaging the in-situ measurements corresponding to the satellite pixels at one-degree spatial resolution. Then the spatiotemporal variability of surface ocean TA is described using monthly and seasonal Level-3 SSS data for the reference year 2014 as well as the global surface ocean TA products.

C. MODEL DESCRIPTION: THE THEORETICAL FORMULATIONS OF TA FOR THE SLR APPROACH

The acid-base chemistry of ocean water is altered by the intake of atmospheric CO_2 and it affects the ocean carbonate

chemistry parameters. TA is an important property to study the calcification and dissolution processes and thus it provides useful context for understanding seawater carbonate chemistry across the ocean. In natural waters, TA is produced by both carbonate (Bicarbonates, HCO_3^- and Carbonate ions, CO_3^{2-}) and non-carbonate (borate, $B(OH)_4$; phosphate, PO_4^{3-}; silicate, $H_2SiO_4^{2-}$; and hydroxide, OH^-) alkalinities.

$$TA = [HCO_3^-] + 2\left[CO_3^{2-}\right] + \left[B(OH)_4\right] + 2\left[PO_4^{3-}\right] + \left[H_2SiO_4^{2-}\right] + [OH^-] - [H^+] \pm \text{minor constituents} \quad (1)$$

The TA is dominated by the bicarbonate and carbonate ions and thus determines the carbonate alkalinity (CA)

$$CA = \left[HCO_3^-\right] + 2\left[CO_3^{2-}\right] \quad (2)$$

Under the normal oceanic conditions, CA is an important property that comprises 96% of TA and 5% of the other contributions. These two chemical constituents (bicarbonate and carbonate) in CA increase and decrease proportionately as the SSS increases and decreases [2]. This dependency indicates a good correlation of TA with SSS in near surface ocean waters, which leads to many regional empirical algorithms. The simple relation is given by

$$TA = f(SSS) \quad (3)$$

This relation allowed to derive some regional-specific linear empirical equations using in-situ data [4], [5], [7]. An expression of such algorithms is given by

$$TA = USSS + V \quad (4)$$

Earlier studies have reported the inconsistencies and inaccuracies in the TA products estimated by these algorithms. To overcome these issues, the present study developed a new empirical algorithm (SLR) using a large number (N = 11952) of quality-controlled OADS in-situ data obtained from the various oceans (such as Atlantic, Pacific, Indian and Southern oceans) with greater spatial and temporal resolutions. The new empirical formulation of this SLR approach is expressed as

$$TA = 49.504SSS + 81.68 \quad (5)$$

Because of the strong linear correlation of TA with SSS, the slope coefficient is close to unity (Fig. 2) which indicates that the SLR algorithm could be more robust and accurate for generating the global TA maps. Although TA showed a close correlation with SSS, there was a slight deviation in the TA-SSS global relationship (Fig. 2) due to the influence of edge case scenarios (nearshore, river mouth and upwelling regions) and other seasonal effects caused by the net community production [4], [21]. The spatiotemporal variability of surface ocean TA fields in these regions was controlled by the influence of other complex physical and biogeochemical parameters such as SST, sea surface current velocity, climatic

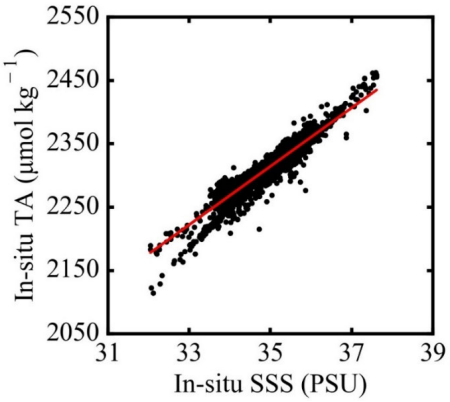

FIGURE 2. A relationship of the OADS in-situ measured TA versus SSS data (N = 11952) from diverse range of oceanic waters (Atlantic, Pacific, Indian and Southern Oceans.)

conditions, dissolved oxygen and nutrients (nitrogen, phosphorous, and silicate concentration) [4].

III. PERFORMANCE ASSESSMENT

The quantitative performance assessment of the SLR algorithm was done using the standard statistical matrices (MRE, MNB, RMSE, R^2, slope and intercept). These statistical parameters are described below

Mean relative error (MRE)

$$= \frac{1}{N}\sum_{i=0}^{N}\frac{\left|(TA^{estimated} - TA^{in-situ})\right|}{TA^{in-situ}} \quad (6)$$

mean normalized bias (MNB)

$$= \frac{\sum_{i=0}^{N}\left(TA^{estimated} - TA^{in-situ}\right)}{N} \quad (7)$$

root mean square error (RMSE)

$$= \sqrt{\frac{\sum_{i=0}^{N}\left(TA^{estimated} - TA^{in-situ}\right)^2}{N}} \quad (8)$$

Residual error (RE)

$$= TA^{in-situ} - TA^{estimated} \quad (9)$$

The slope, intercept and correlation coefficient (R^2) were derived from the regression analysis. These statistical matrices represent the systematic errors (MRE), random errors (RMSE) and deviations (MNB, slope, intercept and R^2) between the in-situ and estimated TA values.

To assess the performance of the present SLR approach in estimating the global TA fields, a large number of samples was considered in this study (N = 27137, which include 16949 samples from the OADS data repository for model development and validation purposes and 10188 samples from the GLODAPv2 dataset for model validation purpose). Based on the spatiotemporal coverage and satellite data availability (as discussed earlier), the OADS in-situ dataset was randomly divided into two datasets – 11952 samples for model development and 4997 samples for model validation. The in-situ dataset used for model development contained

the TA values in the range of 2114-2463 μmol kg^{-1} with a mean of 2309 μmol kg^{-1} and an RMSE deviation of 11.19 μmol kg^{-1}. The in-situ dataset used for model validation (15185 samples, which included 4997 samples from the OADS in-situ data and 10188 samples from the GLODAPv2 in-situ data) contained the TA values in the range of 1746-2468 μmol kg^{-1} with a mean of 2274.62 μmol kg^{-1} and an RMSE deviation of 21.43 μmol kg^{-1} (OADS RMSE deviation: 9.31 μmol kg^{-1}; GLODAPv2 RMSE deviation: 25.34 μmol kg^{-1}).

Overall, the combined in-situ dataset used for both model development and validation purposes contained the TA values in the range of 1746-2468 μmol kg^{-1} with a mean of 2289.79 μmol kg^{-1} and an RMSE deviation of 17.67 μmol kg^{-1}. A slight RMSE deviations in the model development data are owing to an overestimation of TA in Antarctic and Indian Ocean waters and an underestimation of TA in central Indian Ocean waters. The deviations in TA occurred due to the influence of other parameters (nutrients and dissolved oxygen) linked with the large irregular inter-annual variability caused by the El Nino and La Nina events, seasonal variations, and edge case scenarios [4]. The present study did not include these parameters due to the lack of accurate satellite-based models for global ocean applications [21]. The validation and inter-comparison of the present SLR approach with existing TA models are presented in ''Section IV. Results and discussion.''

IV. RESULTS AND DISCUSSION

This section presents the statistical comparison results using in-situ and satellite matchup data and the spatial distribution and temporal variability of satellite-derived TA in global ocean waters.

A. DIRECT AND DERIVED IN-SITU TA VALIDATIONS

To validate the SLR approach, approximately 4997 independent OADS in-situ TA measurements were collected from the different oceanic regions such as Atlantic Ocean (N = 3080), Pacific Ocean (N = 1322), and Indian Ocean (N = 595). In the Atlantic Ocean, the TA estimates from OADS in-situ data (using SLR) agree well with measured data (MRE 0.003, MNB −4.672, RMSE 9.27, Slope 1 and R^2 0.99). The errors are relatively small compared to those of the Millero et al. [5] Atlantic-Ocean regional TA equation (MRE 0.004, MNB −7.728, RMSE 11.89, Slope 1.04 and R^2 0.99). In the Pacific Ocean, SLR produced the improved results (MRE 0.003, MNB 3.025, RMSE 10.40, Slope 1.02 and R^2 0.98) as compared to the Millero et al. [5] regional TA equation (MRE 0.007, MNB −11.876, RMSE 19.22, Slope 1.13 and R^2 0.98). In the Indian Ocean, SLR estimated TA with small errors and high slope and correlation coefficients (MRE 0.002, MNB −0.584, RMSE 6.64, Slope 1.11 and R^2 0.96) when compared to the results from the Millero et al. [5] regional equation (MRE 0.008, MNB −19.025, RMSE 25.71, Slope 1.55 and R^2 0.96). The overall performance of SLR was also excellent considering all the regional OADS in-situ samples (MRE 0.003, MNB −2.149, RMSE 9.31, Slope 1 and R^2 0.99). These results were obtained from the OADS in-situ validation data shown in Fig. 3 (a, e, i, and m) and Table 3.

B. SATELLITE TA VALIDATION

To validate the satellite-derived TA products using in-situ data, the TA estimates from the SLR algorithm based on the satellite SSS products (Aquarius and SMAP) were compared with independent OADS in-situ data. For this analysis, a total of 4997 independent OADS in-situ TA samples were used. Due to cloud coverage, missing scanlines, and missing satellite SSS data, the number of matchup data reduced to 3008. Because the OADS in-situ TA measurements are continuous and the corresponding satellite-based TA are produced at a spatial resolution of 1° × 1° degrees, it was necessary to generate matchup data by converting OADS in-situ observations into the 1° spatial resolution satellite derived TA products. Due to heavy cloud coverage and missing scan lines in the daily satellite derived ocean color products, there were fewer matchup data reported in earlier studies [22]. To overcome this limitation, the present study used eight-day composite binned images of Aquarius SSS products for satellite validation analysis. Similarly, the SMAP daily data files are based on the SSS averages over an 8-day moving time window. Since the temporal variability of SSS is small as compared to the spatial variability [2], the present study did not include the temporal matchup analysis for the purpose to ensure more validation points in the satellite validation. This yielded approximately 522 co-located TA and SSS data samples, of which 290 samples were from the Atlantic Ocean, 106 samples from the Pacific Ocean, and 126 from the Indian Ocean. The independent OADS in-situ (direct and derived) and satellite validations were carried out with these data and the results were compared with the Millero et al. [5] regional algorithm outputs. Figure 3 shows the scatter plots of in-situ (third row) and satellite validation (fourth row) results from the SLR and Millero et al. [5] regional regression equations after the removal of points with no satellite data and binning to 1 degree spatial resolution, whereas figure 4 shows the corresponding line plots (first and second row) and error plots (third and fourth row). Statistical comparison of in-situ and satellite validation results were shown in the Table 4 (A) and Table 4 (B) respectively. Whereas, a global map showing the residual error between in-situ TA versus in-situ derived TA and satellite derived TA data are shown in figure 5 (c&d).

This validation analysis showed a close consistency of the OADS in-situ TA with SLR-derived TA data (MRE 0.002, MNB −0.581, RMSE 8.365, Slope 1.009, R^2 0.98) and satellite-estimated TA data (MRE 0.004, MNB 2.212, RMSE 13.714, Slope 0.941, R^2 0.95). The small errors and high correlation coefficients indicate that the SLR approach is robust in estimating the TA fields in the global oceans with the desired accuracy. As the TA is dependent on the SSS, a comparison of the OADS in-situ SSS data with satellite derived SSS data (from Aquarius and SMAP) was conducted

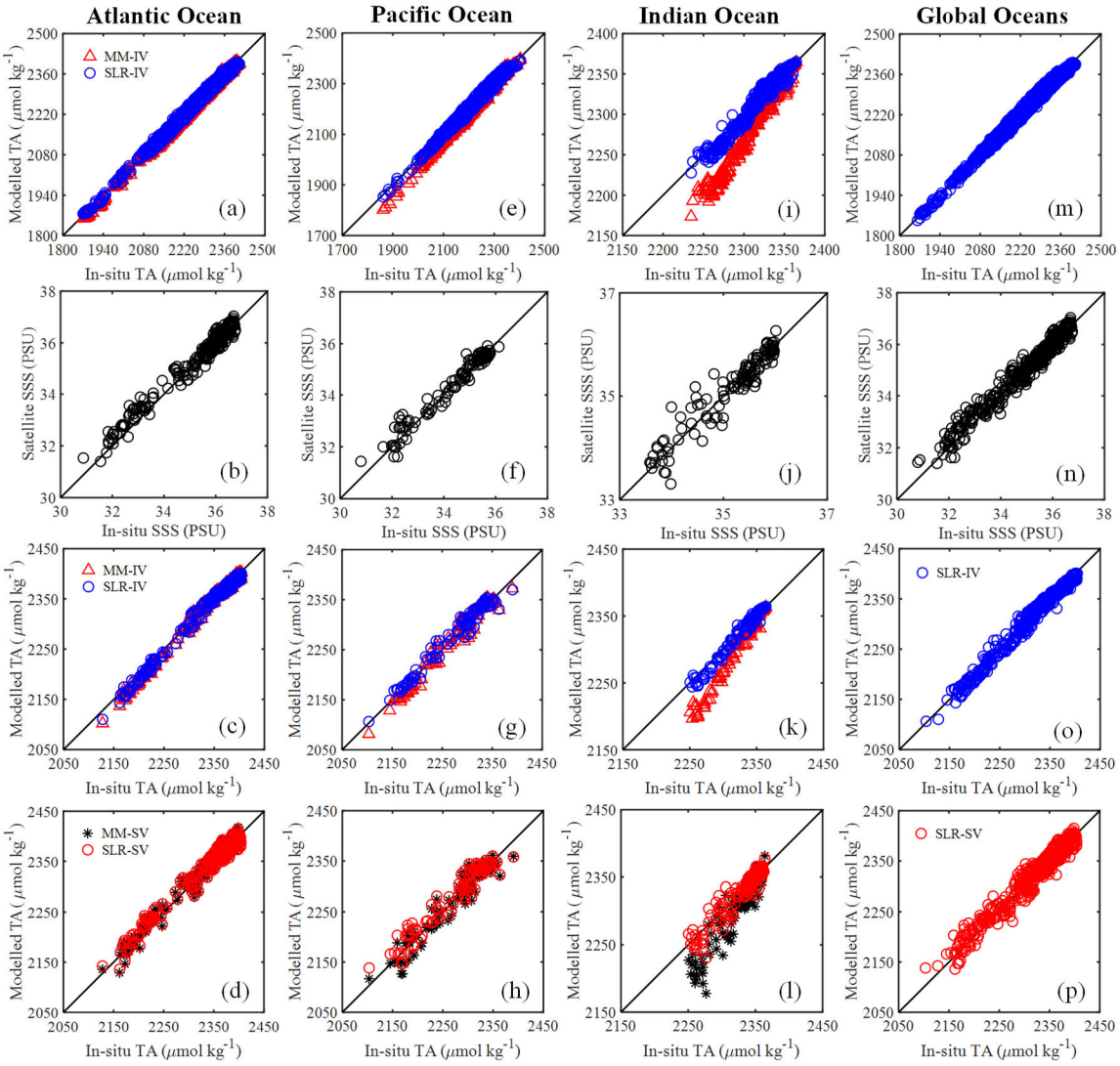

FIGURE 3. The OADS in-situ and satellite validation results based on the data from the Atlantic (a-d), Pacific (e-h), Indian (i-l), and global oceans (m-p). MM-Millero model; SLR-Single Linear Regression (SLR) approach; IV- In-situ validation; ITA- In-situ measured TA; SV – Satellite validation. The global oceans represent the combined (Atlantic, Pacific, and Indian) validation results.

as shown in Fig. 3 (b, f, j, and n), where the in-situ measured SSS agree well with satellite-estimated SSS data as confirmed by the statistical matrices (MRE 0.005, MNB 0.056, RMSE 0.252, Slope 0.93, R^2 0.96). A slight deviation of the satellite-derived SSS could be caused by diurnal SSS fluctuations and the difference between spot OADS in-situ observations and satellite pixel measurements [23], [24]. Table 5 shows the statistical comparison results for the OADS in-situ and satellite-derived SSS data.

C. GLODAP TA VALIDATION

To further examine the accuracy and robustness of the SLR approach, the recently published GLODAPv2 data collected from discrete locations were used (https://www.ncei.noaa.gov/access/ocean-carbon-data system/oceans/GLODAPv2_2021). To include more spatial and temporal coverage in the validation datasets, samples measured at depth <5 m were used for validation analysis. This leads to approximately 10188 samples, which are used to validate the SLR derived TA with in-situ measured GLODAPv2 data. The GLODAPv2 in-situ validation data are a good representation of coastal and open ocean waters, which contain major tropical and subtropical domains, major gyre systems, warming and stratification conditions, mixing and dilution processes, and biological processes in the Atlantic, Pacific and Southern oceans.

The GLODAPv2 in-situ based TA validation results indicated small errors (MRE 0.007, MNB −1.73, and RMSE 25.34 μmol kg^{-1}), a high slope (1.02), and a high correlation coefficient (R^2 0.94). It should be mentioned that some of the GLODAPv2 in-situ measurements come from the edge case scenarios (nearshore, river mouth, and upwelling regions), which lead to a slightly higher RMSE (25.34 μmol

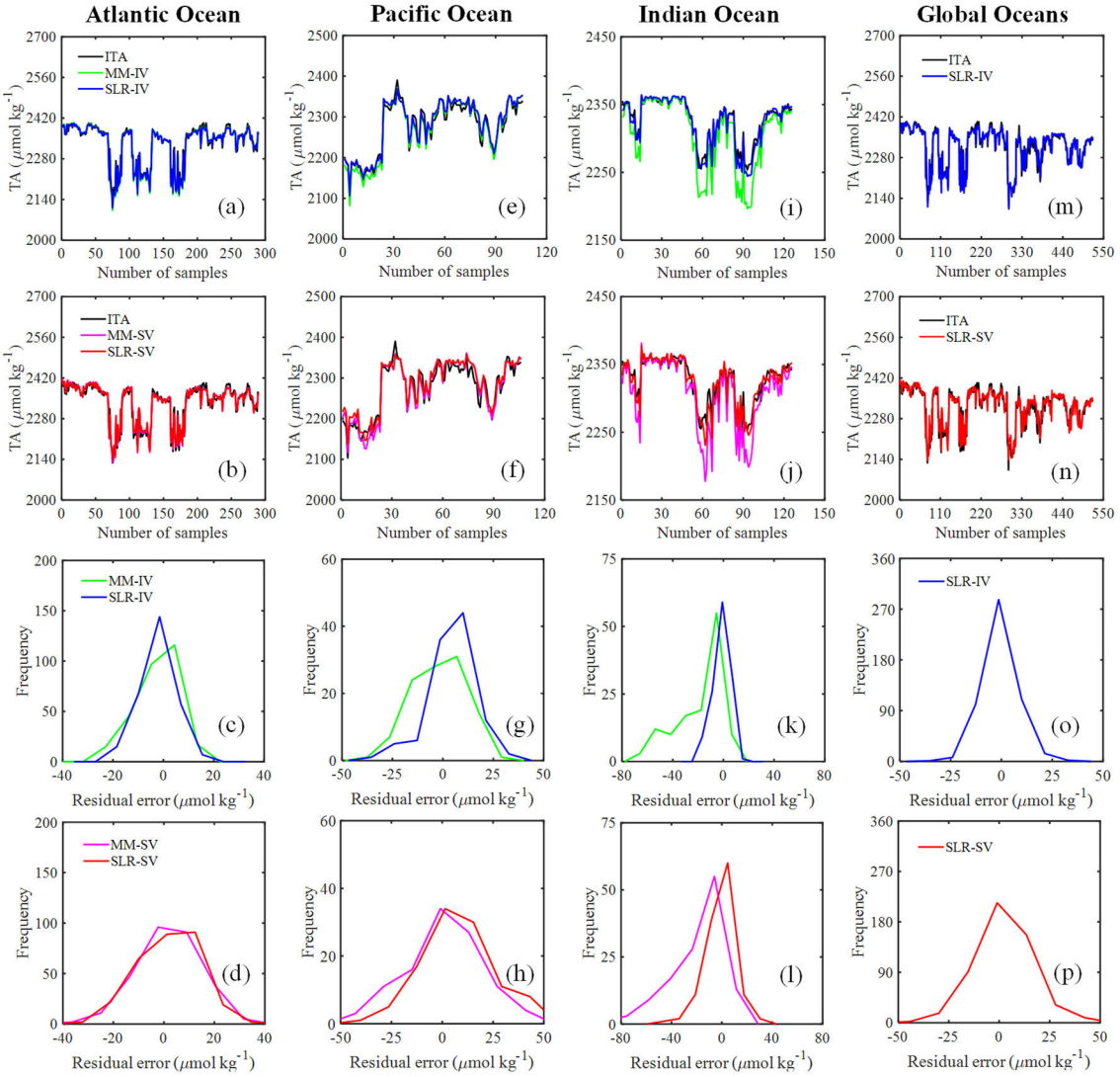

FIGURE 4. The OADS in-situ and satellite validation line plots (first and second rows) and residual error plots (third and fourth rows) based on the data from the Atlantic (a-d), Pacific (e-h), Indian (i-l), and global oceans (m-p). MM-Millero model; SLR-Single Linear Regression (SLR) approach; IV- In-situ validation; and SV – Satellite validation. The global oceans represent the combined (Atlantic, Pacific, and Indian) validation results.

kg^{-1}) deviations. The higher RMSE may be attributed to these facts: i) some of the GLODAPv2 in-situ validation points are located in the equatorial Pacific zone, where the large variation points of surface ocean TA are dominated by eddy mixing, high precipitation and evaporation rates, and the large irregular interannual variability is caused by ocean dynamics during the El Nino and La Nina events [4], ii) Although the seasonal variation of surface ocean TA is very small in the tropical and subtropical regions, large seasonal variations of TA associated with the biological activities in the polar and subpolar regions leads to the large difference of TA up to 30 μmol kg^{-1} [4], and (iii) most of the edge case GLODAPv2 in-situ validation points belong to coastal waters. In such edge cases, the surface ocean TA variations are controlled by the complex processes, such as physical (evaporation and precipitation), biological (photosynthesis and oxidation of organic matter), and non-conservative processes (production and dissolution of $CaCO_3$).These processes are in turn controlled by SST, SSS, dissolved oxygen and nutrients (nitrogen, phosphorous and silicate concentration) [21]. The present study included the edge case scenarios data in the model development and validation datasets, but the related governing control parameters (such as dissolved oxygen and nutrients) are excluded in the model formulations due to the lack of accurate and precise satellite-based models applicable to global oceanic waters.

Further validation was carried out using the global surface ocean TA maps obtained from the GLODAPv2 climatological SSS data (SLR) and direct GLODAPv2 surface ocean TA

TABLE 3. Statistical comparison of the OADS in-situ validation (direct and derived) results from the SLR and Millero et al. [5] regional regression equations.

Region	Model	MRE	MNB	RMSE	SLOPE	INTERCEPT	R^2	N
Atlantic Ocean	Millero et al. [5]	0.004	-7.728	11.89	1.040	-99.116	0.99	3080
	Present Study	0.003	-4.672	9.27	1.005	-16.557	0.99	
Pacific Ocean	Millero et al. [5]	0.007	-11.876	19.22	1.131	-301.59	0.98	1322
	Present Study	0.003	3.025	10.40	1.025	-53.185	0.98	
Indian Ocean	Millero et al. [5]	0.008	-19.025	25.71	1.552	-1301.1	0.96	595
	Present Study	0.002	-0.584	6.64	1.117	-272.47	0.96	
Global Ocean	Present Study	0.003	-2.149	9.31	1.002	-6.727	0.99	4997

TABLE 4. (a). Statistical comparison of the OADS in-situ validation results from the SLR and Millero et al. [5] algorithms. These data were selected after eliminating points with no satellite data and binning to 1-degree spatial resolution. (b) Statistical comparison of the satellite validation (with the OADS in-situ data) results from the SLR and Millero et al. [5] algorithms. These data were selected after eliminating points with no satellite data and binning to 1-degree spatial resolution.

(a)

Region	Model	MRE	MNB	RMSE	SLOPE	INTERCEPT	R^2	N
Atlantic Ocean	Millero et al. [5]	0.002	-2.500	8.695	1.069	-164.73	0.99	290
	Present Study (SLR)	0.002	-2.252	7.387	1.033	-79.949	0.99	
Pacific Ocean	Millero et al. [5]	0.005	-1.676	13.463	1.089	-206.24	0.97	106
	Present Study (SLR)	0.004	5.012	12.046	0.987	33.222	0.97	
Indian Ocean	Millero et al. [5]	0.007	-17.968	26.251	1.557	-1313.7	0.98	126
	Present Study (SLR)	0.002	-1.441	6.501	1.120	-281.54	0.98	
Global Ocean	Present Study (SLR)	0.002	-0.581	8.365	1.009	-23.43	0.98	522

(b)

Region	Model	MRE	MNB	RMSE	SLOPE	INTERCEPT	R^2	N
Atlantic Ocean	Millero et al. [5]	0.004	1.924	12.272	0.978	52.583	0.96	290
	Present Study (SLR)	0.004	2.022	12.357	0.945	130	0.96	
Pacific Ocean	Millero et al. [5]	0.006	0.722	18.118	1.019	-43.875	0.92	106
	Present Study (SLR)	0.006	7.186	18.526	0.923	180.35	0.92	
Indian Ocean	Millero et al. [5]	0.008	-18.100	28.311	1.458	-1084.3	0.89	126
	Present Study (SLR)	0.003	-1.536	11.790	1.049	-116.49	0.89	
Global Ocean	Present Study (SLR)	0.004	2.212	13.714	0.941	138.44	0.95	522

climatological data, which were used to generate the residual error (Fig. 9) and histogram plots (Fig.10). Figure 9 demonstrates the spatiotemporal comparison of the SLR-derived TA with GLODAPv2 data. This comparison shows that the SLR-derived TA structures are closely consistent with GLODAPv2 data with an RMSE deviation of 10-30 μmol kg^{-1}. A small deviation between these two datasets could come from the difference/ inconsistency in the SSS climatological data and direct GLODAPv2 climatological data.

TABLE 5. Statistical comparison results for the OADS in-situ and satellite-derived SSS data.

Ocean region	MRE	MNB	RMSE	Slope	R^2	N
Atlantic	0.005	0.086	0.259	0.913	0.97	290
Pacific	0.005	0.043	0.266	0.936	0.95	106
Indian	0.004	-0.001	0.220	0.935	0.90	126
Overall	0.005	0.056	0.252	0.929	0.96	522

TABLE 6. Regional- and global-scale empirical surface ocean TA approaches.

Author	Region	Parameters	N
Bates et al. [14]	Indian Ocean	SST, SSS, Depth, AOU, Latitude, Ni and P.	2363
McNeil et al. [13]	Southern Ocean	SSS, Ni and Si	1200
Arrigo et al. [12]	Arctic Ocean	SST, SSS	853
Millero et al. [5]	Global	SSS	1740
Lee et al. [3]	Global	SST, SSS	5692
Present study	Global	SSS	11952

N: number of in-situ measurements, SST: sea surface temperature, SSS: sea surface salinity, AOU: apparent oxygen utilization, Ni: nitrate (no_3^-), P: phosphate (po_4^{3-}) and Si: silicate (sio_4) concentrations.

1) INTER-COMPARISON OF THE EXISTING GLOBAL TA STUDIES USING THE GLODAPv2 DATA

To examine the performance of SLR in producing the precise global surface ocean TA fields and their in-comparison with the past TA studies, two global empirical formulations for TA as proposed by Lee et al. [3] and Takahashi et al. [4] were considered in this work. Lee et al. [3] classified the global oceans into five ocean regimes according to the latitude and longitude and SST and SSS fields. Based on the range of SST and SSS, they categorized the surface ocean TA data (depth $<$ 30m) and derived an empirical formulation to estimate regional TA fields as a quadratic function of the SST and SSS for each ocean regime. The results of these regional empirical formulations were compared with those of the SLR approach using 21826 samples (depth $<$ 30m) obtained from the GLODAPv2 in-situ dataset. Table 7 shows the statistical comparison results for the SLR and Lee et al. [3] approaches. Note that the SLR yielded similar statistical values (MRE 0.398, RMSE 10.94, and R^2 0.94) as the Lee et al. [3] formulation (MRE 0.365, RMSE 11.42, and R^2 0.93) but with global and regional applicability.

Similarly, Takahashi et al. [4] divided the global oceans into 33 regions and derived a linear empirical equations to estimate surface ocean TA (depth $<$ 50 m) as a function of the SSS for 27 of the regions. For evaluating the SLR and Takahashi et al. [4] approaches, a total of 42306 samples (depth $<$ 50m) from the GLODAPv2 in-situ dataset were used. Table 8 shows the statistical comparison results for the SLR and Takahashi et al. [4] equations. Although the results

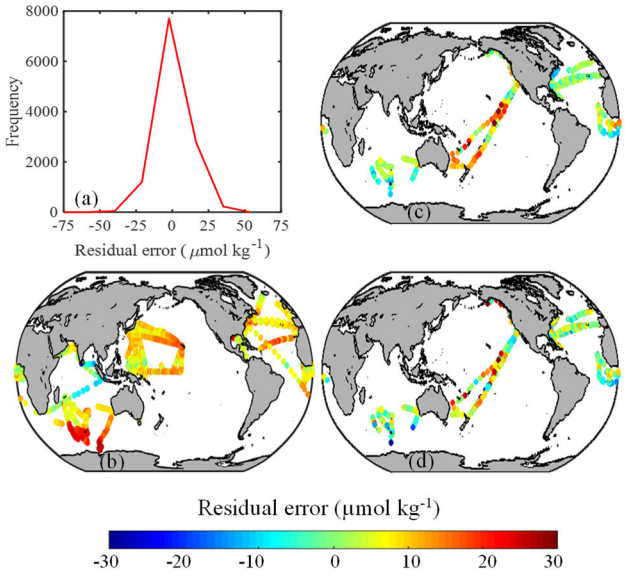

FIGURE 5. Residual errors in the OADS in-situ calibration data (Left panels: (a) histogram plot, and (b) in-situ derived TA) and validation data (Right panels: (c) in-situ derived TA, and (d) satellite derived TA.)

are slightly improved by the Takahashi et al. [4] formulation in certain regional waters, its global applicability was reduced as the SLR estimated the global TA fields more accurately than their algorithm (MRE 0.701, MNB −0.168, RMSE 17.82, and R^2 0.88 for SLR approach; MRE 0.786, MNB 0.532, RMSE 21.17, and R^2 0.88 for the Takahashi et al. [4] formulation.

D. SPATIOTEMPORAL VARIABILITY OF GLOBAL SURFACE OCEAN TA

A detailed knowledge of the spatiotemporal variability of the global surface ocean TA is crucial for understanding the global ocean carbon cycle, acidification, and other carbonate chemistry dynamics in the ocean. The surface ocean TA varies depending on the various physical, biological, and chemical processes which determine the concentrations of the ocean chemical constituents (carbonate, bicarbonate, phosphate, silicate and other minor constituents). The increase or decrease of these chemical constituents' contents is directly proportional to the SSS variations as there is a strong linear correlation between the ocean SSS and TA fields [2], [3], [4], [5], [19]. Also, the spatial variability of TA and SSS is greater than their temporal variability in most oceanic waters. For example the TA fields exhibit less variation in the Southern Hemisphere than in the Northern Hemisphere due to the reduced SSS variation [2].

The spatial distribution and temporal variation of TA and SSS in global and regional ocean waters produced by SLR are shown in Figs. 6 & 7 for the reference year 2014. There were three primary reasons for selecting the reference year 2014; (i) The availability of independent in-situ TA validation data, (ii) The availability of in-situ and satellite-based

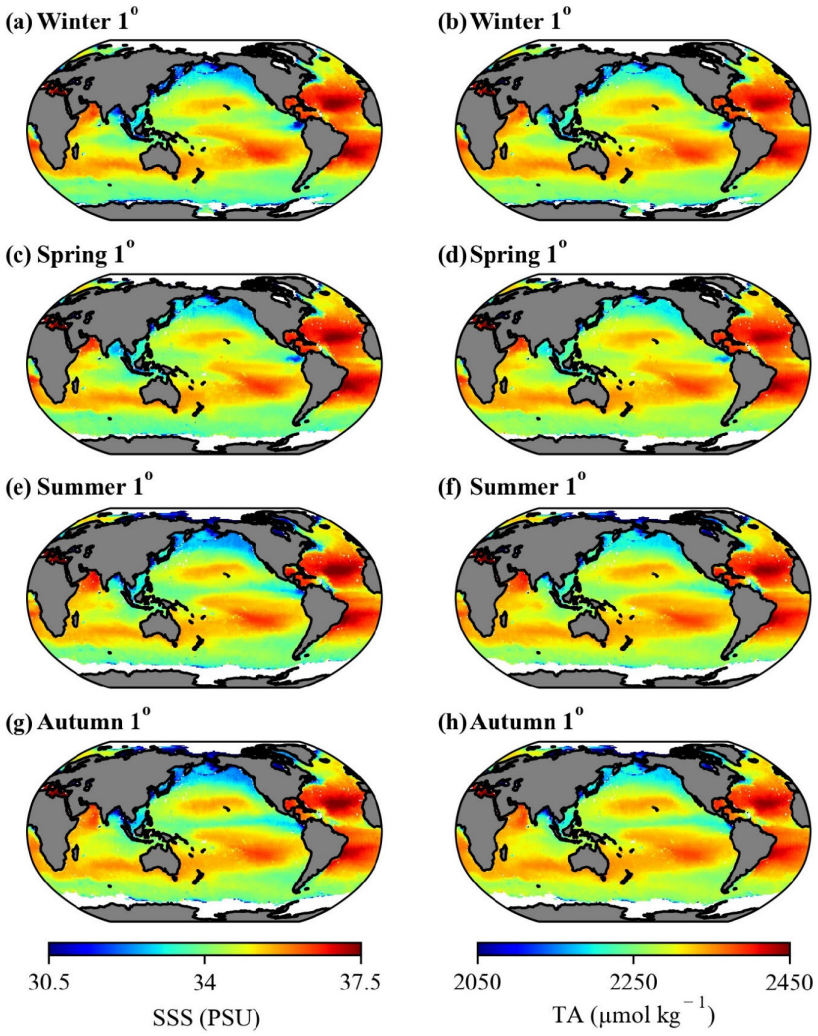

FIGURE 6. Global maps of Aquarius Level-3 SSS and the corresponding satellite-derived TA data at 1° × 1° spatial resolution for four seasons: Winter (a and b, January-March), Spring (c and d, April-June), Summer (e and f, July-September), and Autumn (g and h, October-December) for the reference year 2014.

climatological TA maps for the reference year 2014 (for the purpose of graphical inter-comparison with the previous studies on the global ocean TA [2], [4]), and (iii) Krishna et al. [24] recently published a study that demonstrated the spatiotemporal variability of partial pressure of carbon dioxide (pCO_2) fields (monthly and seasonal) for the reference year 2014, which motivated us to conduct a similar study and produce global TA fields for this reference year.

In the equatorial region, TA is less than 2300 μmol kg^{-1} and displays less variation like SSS due to heavy precipitation events. In stratified tropical and subtropical ocean regions (Fig. 6), TA (>2300) increases to a maximum value like SSS due to excessive annual evaporation events. Such high evaporative ocean regions within the subtropical gyres are characterized by very high TA (>2450) and SSS and the Atlantic subtropical gyres are highest of the other subtropical regions. Figure 6 (b, d, f and h) shows the subtropical regions of the North and South Atlantic with the highest TA (compared to other global ocean regions) and SSS as the result of the high evaporation to precipitation (E/P) ratios [2], [3], [5].

In polar and subpolar regions, seasonal TA variation is maximum due to the E/P ratio. The seasonal variations of TA in polar and subpolar regions (Fig. 6) are corroborated by the earlier studies. The seasonal variability of TA in surface ocean waters is a complex interplay of physical, chemical and biological factors. It is important to increase our understanding of this variability to predict the impact of climate change on ocean chemistry and global carbon cycle. It should be noted that TA exhibits the relatively low seasonal and inter annual variability within the seawater CO_2 chemistry system [2], [3], [4], [19], [25]. However, it is crucial to monitor and account for these changes due to the significant role of TA in oceanic anthropogenic carbon storage and its

TABLE 7. Statistical GLODAPv2 in-situ comparison results from the SLR and Lee et al. [3] regional regression equations. To be consistent with the surface layer defined in Lee et al. [3], samples measured at depths <30 m were considered for this inter-comparison analysis. L-06 depicts the Lee et al. [3] equation.

	MRE		MNB		RMSE		R^2		N
Regions	L-06	SLR	L-06	SLR	L-06	SLR	L-06	SLR	
North Atlantic	0.243	0.443	-0.015	0.117	8.52	11.97	0.97	0.98	2785
North Pacific	0.244	0.381	0.048	0.205	7.31	10.01	0.93	0.94	708
Equatorial upwelling Pacific	0.331	0.334	0.095	0.109	9.80	9.79	0.96	0.96	9424
Subtropics	0.750	0.520	-0.307	-0.157	23.86	14.22	0.83	0.90	5552
Southern Ocean	0.258	0.312	0.085	0.001	7.63	8.73	0.93	0.93	3357
Overall mean	0.365	0.398	-0.018	0.055	11.42	10.94	0.93	0.94	21826

TABLE 8. Statistical GLODAPv2 in-situ comparison results from the SLR and Takahashi et al. [4] regional regression equations. To be consistent with the surface layer defined in Takahashi et al. [4], samples measured at depths <50 m were considered for this inter-comparison analysis. T-14 depicts the Takahashi et al. [4] equation.

	MRE		MNB		RMSE		R^2		N
Regions	T-14	SLR	T-14	SLR	T-14	SLR	T-14	SLR	
West GIN Seas	0.656	0.499	0.138	0.207	26.40	14.36	0.87	0.87	595
East GIN Seas	0.369	0.307	0.130	0.085	10.55	9.01	0.81	0.81	739
High Arctic	1.081	0.923	0.848	-0.485	36.29	23.82	0.94	0.94	949
Beaufort Sea	1.561	1.138	1.271	-0.921	38.93	26.29	0.98	0.98	1122
Labrador Sea	1.247	0.494	1.243	-0.054	32.13	13.55	0.95	0.95	1628
Subarctic Atlantic	0.450	0.326	0.384	0.175	12.01	9.17	0.89	0.89	3511
North Atlantic Drift	0.305	0.270	0.230	0.134	8.79	7.98	0.92	0.92	2243
Central Atlantic	0.318	0.289	0.202	-0.010	9.27	8.75	0.96	0.96	7516
South Atlantic Transition Zone	0.583	0.388	0.555	-0.373	14.64	10.59	0.85	0.85	270
Antarctic (Atlantic)	0.893	2.044	0.888	-2.044	21.92	47.97	0.76	0.76	997
Kuroshio-Alaska Gyre	2.683	0.567	2.683	-0.149	63.58	15.09	0.88	0.88	4865
North Central Pacific	1.002	0.392	0.220	0.030	29.95	10.61	0.94	0.94	1963
Okhotsk Sea	0.747	1.208	0.747	-1.208	17.23	27.21	0.97	0.97	23
Central Tropical North Pacific	1.274	0.831	-1.077	0.056	38.76	21.08	0.76	0.76	18
Tropical East North Pacific	0.961	0.710	0.748	0.671	23.48	17.57	0.85	0.85	3197
Panama Basin	0.306	0.871	-0.284	0.871	10.29	21.44	0.56	0.56	7
Central South Pacific	0.328	0.498	0.134	0.254	9.43	13.35	0.93	0.93	3327
East Central South Pacific	0.307	0.343	0.158	-0.157	9.03	9.66	0.95	0.95	317
Subpolar South Pacific	0.323	0.324	0.279	0.280	9.54	9.48	0.91	0.91	628
Antarctic (Pacific)	1.034	1.247	1.034	-1.247	24.28	28.77	0.93	0.93	813
Main North Indian	0.364	0.728	-0.057	0.702	12.24	19.42	0.98	0.98	767
Red Sea	0.596	0.419	0.589	0.379	18.88	13.27	0.74	0.74	44
Bengal Basin	0.251	0.582	-0.001	0.475	7.19	15.53	0.93	0.93	110
Main South Indian	0.201	0.574	-0.024	0.548	6.15	15.35	0.95	0.95	2708
South Indian Transition	0.607	0.508	0.557	-0.332	16.14	15.13	0.85	0.85	988
Antarctic (Indian)	1.493	1.213	1.493	-1.213	34.54	28.25	0.80	0.80	1174
Circumpolar Southern Ocean	1.278	1.224	1.278	-1.224	30.06	28.49	0.83	0.83	1742
Overall mean	0.786	0.701	0.532	-0.168	21.17	17.82	0.88	0.88	42306

ability to buffer changes in seawater potential of hydrogen (pH) concentration.

The magnitudes of TA are high in Arabian Sea waters due to the upwelling process and low in Bay of Bengal waters

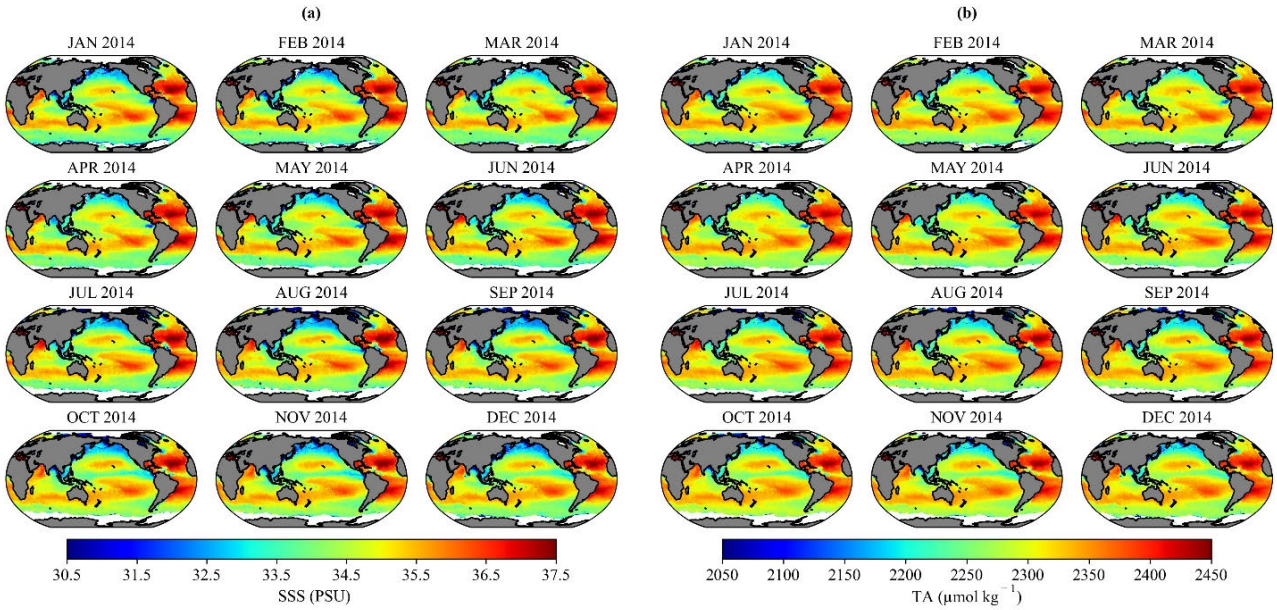

FIGURE 7. Spatiotemporal variability of global monthly surface ocean (a) SSS and (b) TA at 1° × 1° spatial resolution for the reference year 2014.

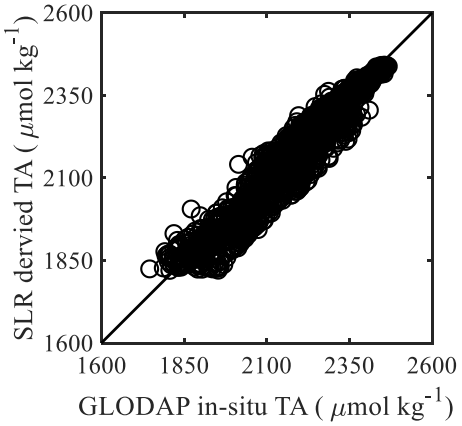

FIGURE 8. Comparison of the TA estimates from SLR with GLODAPv2 in-situ surface ocean discrete data (N = 10188) obtained from the samples at depths <5 m (considered for the validation analysis).

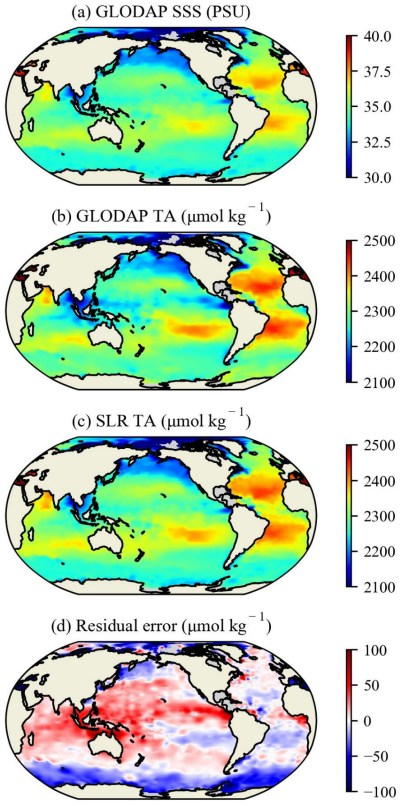

FIGURE 9. Spatiotemporal variability of the global surface ocean climatology of (a) GLODAPv2 SSS, (b) GLODAPv2 TA, (c) SLR TA, and (d) Residual error at 1° × 1° spatial resolution for the period 1972-2020.

due to the freshwater inputs [26], [27]. The surface ocean TA ranged from 2250 to 2500 μmol kg^{-1} in Atlantic Ocean waters, 2100 to 2400 μmol kg^{-1} in Pacific Ocean waters, and 2200 to 2380 μmol kg^{-1} in Southern and Indian Ocean waters (Fig. 6). These spatiotemporal magnitudes of TA as estimated by the SLR approach are well consistent with the previous studies [3], [4], [5], [19].

Furthermore, the TA fields (generated by the present SLR approach) were compared with the in-situ based climatological TA maps of Takashi et al. [4] and satellite based TA maps of Fine et al. [2]. In general, the spatial patterns of the global surface ocean TA fields of the present study are closely consistent with those of Takashi et al. [4] and Fine et al. [2] with a little difference of about 10 to 25 μmol kg^{-1}.

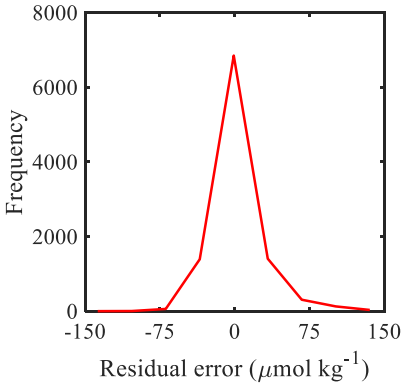

FIGURE 10. The residual error calculated between the in-situ measured GLODAPv2 data and the corresponding SLR derived TA data.

V. CONCLUSION

A simple and straightforward algorithm was developed based on SLR approach and rigorously validated with the regional and global in-situ data and its relative merits was assessed by comparison with the results from three existing algorithms. The results showed the global applicability and robustness of the SLR approach when compared to the existing algorithms in estimating surface ocean TA fields in the regional and global oceans. The SLR algorithm can produce the spatial (basin/global scale) and temporal (daily/monthly/seasonal/annual) resolution TA global maps without involving a smoothing technique across latitudes and longitudes and ocean basins. The SLR algorithm could become a promising tool to estimate global surface ocean TA fields, which would further enhance our present understanding of the global carbon cycle, air-sea CO_2 fluxes, ocean acidification and other carbonate chemistry parameters. Moreover, the global surface ocean pCO_2 and pH fields can be estimated from the inorganic carbonate chemistry calculations with the inputs of TA and dissolved inorganic carbon (DIC) data. The global surface ocean TA and pCO_2 [24] with certain input/output boundary conditions (SST, SSS, pressure and phosphate concentrations) are necessary for estimating the surface DIC, pH, saturation states of calcite and aragonite, and other carbonate chemistry parameters. The error in the SLR-based TA estimates is significantly small and could be influenced by the underlying physical and biogeochemical processes (upwelling, formation and destruction of organic matter, and cold regimes in the polar oceans) especially in high nutrient regions [28]. Our future work would aim to improve the spatiotemporal accuracy in ocean surface TA estimates by using more regional-specific in-situ data collected from the diverse oceanic regimes.

ACKNOWLEDGMENT

The authors would like to thank the Oceanographic section of NASA-GSFC for the support of the SeaDAS software and distribution of the Aquarius and the NASA-JPL for the distribution of the SMAP data, also would like to thank all the scientists, chief scientists, and other individuals, who have collected, processed, quality controlled, and contributed the available in-situ measured data to the NOAA-NCEI database, also would like to thank the anonymous reviewers for their valuable feedback and comments on this work, and also would like to thank their time and expertise in reviewing their work. Their constructive criticism and insightful suggestions have greatly improved the quality of this manuscript.

REFERENCES

[1] R. A. Feely, "Impact of anthropogenic CO_2 on the $CaCO_3$ system in the oceans," *Science*, vol. 305, no. 5682, pp. 362–366, Jul. 2004.

[2] R. A. Fine, D. A. Willey, and F. J. Millero, "Global variability and changes in ocean total alkalinity from aquarius satellite data," *Geophys. Res. Lett.*, vol. 44, no. 1, pp. 261–267, Jan. 2017.

[3] K. Lee, L. T. Tong, F. J. Millero, C. L. Sabine, A. G. Dickson, C. Goyet, G.-H. Park, R. Wanninkhof, R. A. Feely, and R. M. Key, "Global relationships of total alkalinity with salinity and temperature in surface waters of the world's oceans," *Geophys. Res. Lett.*, vol. 33, no. 19, Oct. 2006.

[4] T. Takahashi, S. C. Sutherland, D. W. Chipman, J. G. Goddard, C. Ho, T. Newberger, C. Sweeney, and D. R. Munro, "Climatological distributions of pH, pCO_2, total CO_2, alkalinity, and $CaCO_3$ saturation in the global surface ocean, and temporal changes at selected locations," *Mar. Chem.*, vol. 164, pp. 95–125, Aug. 2014.

[5] F. J. Millero, K. Lee, and M. Roche, "Distribution of alkalinity in the surface waters of the major oceans," *Mar. Chem.*, vol. 60, nos. 1–2, pp. 111–130, Feb. 1998.

[6] W. S. Broecker and T. H. Peng, "Tracers in the sea," in *Lamont-Doherty Observation*. Palisades, NY, USA: Springer, 1982.

[7] V. V. S. S. Sarma, "Monthly variability in surface $pCO_2$and net air-sea CO_2flux in the Arabian sea," *J. Geophys. Res.*, vol. 108, no. C8, p. 3255, 2003.

[8] V. V. S. S. Sarma et al., "Basin-scale pCO_2 distribution using satellite sea surface temperature, Chl a, and climatological salinity in the North Pacific in spring and summer," *Global Biogeochem. Cycles*, vol. 20, no. 3, pp. 1–13, Sep. 2006.

[9] W.-J. Cai, X. Hu, W.-J. Huang, L.-Q. Jiang, Y. Wang, T.-H. Peng, and X. Zhang, "Alkalinity distribution in the western North Atlantic Ocean margins," *J. Geophys. Res.*, vol. 115, no. C8, Aug. 2010.

[10] N. Lefèvre, D. Diverrès, and F. Gallois, "Origin of CO_2 undersaturation in the western tropical Atlantic," *Tellus B*, vol. 62, no. 5, pp. 595–607, Nov. 2010.

[11] Y. Takatani, K. Enyo, Y. Iida, A. Kojima, T. Nakano, D. Sasano, N. Kosugi, T. Midorikawa, T. Suzuki, and M. Ishii, "Relationships between total alkalinity in surface water and sea surface dynamic height in the Pacific ocean," *J. Geophys. Res., Oceans*, vol. 119, no. 5, pp. 2806–2814, May 2014.

[12] K. R. Arrigo, S. Pabi, G. L. van Dijken, and W. Maslowski, "Air-sea flux of CO_2 in the Arctic ocean, 1998–2003," *J. Geophys. Res.*, vol. 115, no. G4, pp. 1998–2003, Nov. 2010.

[13] B. I. McNeil, N. Metzl, R. M. Key, R. J. Matear, and A. Corbiere, "An empirical estimate of the Southern ocean air-sea CO_2 flux," *Global Biogeochemical Cycles*, vol. 21, no. 3, pp. 11–19, Sep. 2007.

[14] N. R. Bates, A. C. Pequignet, and C. L. Sabine, "Ocean carbon cycling in the Indian ocean: 1. spatiotemporal variability of inorganic carbon and air-sea CO_2 gas exchange," *Global Biogeochemical Cycles*, vol. 20, no. 3, pp. 15–20, Sep. 2006.

[15] K. Friis, A. Körtzinger, and D. W. R. Wallace, "The salinity normalization of marine inorganic carbon chemistry data," *Geophys. Res. Lett.*, vol. 30, no. 2, pp. 1–4, Jan. 2003.

[16] W. T. Liu and X. Xie, "Space observation of carbon dioxide partial pressure at ocean surface," *IEEE J. Sel. Topics Appl. Earth Observ. Remote Sens.*, vol. 10, no. 12, pp. 5472–5484, Dec. 2017.

[17] T. P. Sasse, B. I. McNeil, and G. Abramowitz, "A novel method for diagnosing seasonal to inter-annual surface ocean carbon dynamics from bottle data using neural networks," *Biogeosciences*, vol. 10, no. 6, pp. 4319–4340, Jun. 2013.

[18] B. R. Carter, R. A. Feely, N. L. Williams, A. G. Dickson, M. B. Fong, and Y. Takeshita, "Updated methods for global locally interpolated estimation of alkalinity, pH, and nitrate," *Limnology Oceanography: Methods*, vol. 16, no. 2, pp. 119–131, Feb. 2018.

[19] D. Broullón, F. F. Pérez, A. Velo, M. Hoppema, A. Olsen, T. Takahashi, R. M. Key, T. Tanhua, M. González-Dávila, E. Jeansson, A. Kozyr, and S. M. A. C. van Heuven, "A global monthly climatology of total alkalinity: A neural network approach," *Earth Syst. Sci. Data*, vol. 11, no. 3, pp. 1109–1127, Jul. 2019.
[20] L. Gregor and N. Gruber, "OceanSODA-ETHZ: A global gridded data set of the surface ocean carbonate system for seasonal to decadal studies of ocean acidification," *Earth Syst. Sci. Data*, vol. 13, no. 2, pp. 777–808, Mar. 2021.
[21] P. E. Land, H. S. Findlay, J. D. Shutler, I. G. C. Ashton, T. Holding, A. Grouazel, F. Girard-Ardhuin, N. Reul, J.-F. Piolle, B. Chapron, Y. Quilfen, R. G. J. Bellerby, P. Bhadury, J. Salisbury, D. Vandemark, and R. Sabia, "Optimum satellite remote sensing of the marine carbonate system using empirical algorithms in the global ocean, the greater caribbean, the Amazon plume and the bay of Bengal," *Remote Sens. Environ.*, vol. 235, Dec. 2019, Art. no. 111469.
[22] Y. Bai, W.-J. Cai, X. He, W. Zhai, D. Pan, M. Dai, and P. Yu, "A mechanistic semi-analytical method for remotely sensing sea surface pCO_2 in river-dominated coastal oceans: A case study from the east China sea," *J. Geophys. Research: Oceans*, vol. 120, no. 3, pp. 2331–2349, Mar. 2015.
[23] K. Drushka, S. T. Gille, and J. Sprintall, "The diurnal salinity cycle in the tropics," *J. Geophys. Res., Oceans*, vol. 119, no. 9, pp. 5874–5890, Sep. 2014.
[24] K. V. Krishna, P. Shanmugam, and P. V. Nagamani, "A multiparametric nonlinear regression approach for the estimation of global surface ocean pCO_2 using satellite oceanographic data," *IEEE J. Sel. Topics Appl. Earth Observ. Remote Sens.*, vol. 13, pp. 6220–6235, 2020.
[25] K. Priyanka, R. Shanthi, D. Poornima, A. Saravanakumar, R. Roy, and P. V. Nagamani, "Long-term variability of satellite derived total alkalinity in the southwest bay of Bengal," *Quaternary Sci. Adv.*, vol. 8, Oct. 2022, Art. no. 100066.
[26] D. Sengupta, G. N. Bharath Raj, and S. S. C. Shenoi, "Surface freshwater from bay of Bengal runoff and Indonesian throughflow in the tropical Indian ocean," *Geophys. Res. Lett.*, vol. 33, no. 22, pp. 1–5, 2006.
[27] X. Yi, B. Hänicke, and E. Zorita, "Evolution of the Arabian sea upwelling from the last millennium to the future as simulated by Earth system models," *Climate*, vol. 9, no. 5, p. 72, Apr. 2021.
[28] H.-C. Kim, K. Lee, and W. Choi, "Contribution of phytoplankton and bacterial cells to the measured alkalinity of seawater," *Limnology Oceanogr.*, vol. 51, no. 1, pp. 331–338, Jan. 2006.

KANDE VAMSI KRISHNA received the B.Tech. degree in electronics and communication engineering (ECE) from the Rajiv Gandhi University of Knowledge Technologies (RGUKT), IIIT Nuzvid, Andhra Pradesh, India, in 2015, and the M.Tech. degree in remote sensing from Jawaharlal Nehru Technological University (JNTU), Kakinada, Andhra Pradesh, in 2017. He is currently pursuing the Ph.D. degree with the Department of Ocean Engineering, IIT Madras, Chennai, India. His research interests include satellite oceanography and the development of algorithms for retrieving useful information from satellite observations.

PALANISAMY SHANMUGAM received the Ph.D. degree in optical/microwave remote sensing techniques from Anna University, Chennai, India, in 2002.

He is currently a Professor/a National Geospatial Chair Professor with the Department of Ocean Engineering, IIT Madras, Chennai. He has been a principal investigator of several projects funded by the Government of India. His research interests include ocean optics and imaging, satellite oceanography, radiative transfer in the ocean, algorithm/model development, and underwater wireless optical communication.